*metals*

MDPI

*Article*

# Effect of Temperature and NaClO on the Corrosion Behavior of Copper in Synthetic Tap Water

**Fei Sun, Na Zhang, Shen Chen and Moucheng Li ***

Institute of Materials, School of Materials Science and Engineering, Shanghai University, 149 Yanchang Road, Shanghai 200072, China; 15333588951@163.com (S.C.)
* Correspondence: mouchengli@shu.edu.cn

**Abstract:** The corrosion behavior of copper was investigated in synthetic tap water with and without sodium hypochlorite (NaClO) at different temperatures during immersion for 70 d by using scanning electron microscopy (SEM), X-ray diffraction (XRD), and electrochemical measurement techniques. The weight loss corrosion rate and pit depth of copper first increase and then decrease with the change in solution temperature from 25 to 80 °C. This is mainly related to the corrosion products formed on the copper surface. The main corrosion products change from $Cu_2O$ and $Cu_2(OH)_2CO_3$ to CuO with the increase in solution temperature. The presence of 3 ppm NaClO slightly increases the weight loss corrosion rate and pit depth of copper under all temperatures except for 50 °C and reduces the temperature of the maximum corrosion rate from 50 to 40 °C. Free chlorine reduction accelerates the cathodic reaction of the corrosion process.

**Keywords:** copper; corrosion; tap water; temperature; NaClO

## 1. Introduction

Copper and copper alloys are often used as pipes in heat exchangers due to their excellent machinability, thermal conductivity, weldability, and corrosion resistance [1]. In general, copper pipes undergo insignificant corrosion in pure water [2–4], but corrosion causes damage, such as pitting corrosion in tap water with aggressive ions [5,6]. As one of the important components in gas water heaters, copper heat exchangers often suffer from perforation failure.

Copper heat exchangers usually operate at room temperature to about 80 °C. Water temperature is an important factor for the corrosion resistance of copper pipes. There are many reports about the influence of temperature on the corrosion behavior of copper [6–9]. Rahman et al. [7] studied the corrosion of copper heat exchangers in river water and seawater at different temperatures for 30 d. They found that the corrosion rate and ion conductivity increase with the solution temperature from 20 to 80 °C. Ren et al. [8] studied the effect of dissolved oxygen in tap water on copper corrosion under temperatures of 30 to 50 °C. The increase in temperature results in a lower oxygen solubility and a larger oxygen diffusion coefficient, which produces the highest corrosion rate at about 40 °C for copper. Cai et al. [9] reported that the corrosion rate of the copper alloy B10 in seawater noticeably decreases with the change in temperature from 25 to 60 °C due to the reduction in dissolved oxygen by about 39%. Lytle et al. [6] found that the copper pipelines of their testing community showed pitting leakage in cold water, but almost no leakage in hot water.

NaClO is usually added to the tap water system for disinfection [10]. According to the Chinese standard GB 5749-2022 (i.e., Hygienic Standard for Drinking Water) [11], the limit concentration of chlorine in tap water is 2 mg $L^{-1}$. Free chlorine may have a significant impact on the corrosion of copper in domestic water. The cathodic reaction on the surface of copper in natural and drinking water is generally dominated by oxygen reduction. Under

check for updates

**Citation:** Sun, F.; Zhang, N.; Chen, S.; Li, M. Effect of Temperature and NaClO on the Corrosion Behavior of Copper in Synthetic Tap Water. *Metals* **2024**, *14*, 543. https://doi.org/10.3390/met14050543

Academic Editor: Belén Díaz Fernández

Received: 16 April 2024
Revised: 28 April 2024
Accepted: 30 April 2024
Published: 3 May 2024

**Copyright:** © 2024 by the authors. Licensee MDPI, Basel, Switzerland. This article is an open access article distributed under the terms and conditions of the Creative Commons Attribution (CC BY) license (https://creativecommons.org/licenses/by/4.0/).

the conditions of ambient temperature and pH of drinking water (usually between 6.5 and 8.5), hypochlorite mainly exists as hypochlorite (HClO) and hypochlorite ions ($ClO^-$) in the solution [12,13]. Compared with oxygen reduction, chlorine reduction occurs at a higher theoretical oxidation/reduction potential, which can increase the mixed electrode potential of the corrosion system [14–16]. In chlorinated tap water, free chlorine will take part in the cathodic reaction process and affect the corrosion rate of copper pipes [12,17–20]. Montes et al. [12] observed the occurrence of pitting corrosion for copper after 4 weeks of dynamic immersion in tap water at 50 °C by increasing the NaClO concentration from 1 to 25 ppm. Atlas et al. [17] found that NaClO may accelerate the dissolution of a copper tube in static tap water. Boulay et al. [18] found that the addition of 0.7 mg $L^{-1}$ NaClO increases the soluble copper content in soft water at pH 9.5. Yohai et al. [19] found that the passive film on a brass surface becomes more porous and less protective by adding NaClO into tap water. Tzevelekou et al. [20] found that the pitting corrosion leakage of copper water pipes after 6 years of service is related to the high chlorine content from NaClO disinfection treatment.

At present, there is still insufficient understanding about the effect of temperature and NaClO on the corrosion of copper in tap water. In this work, the corrosion behavior of copper was studied in synthetic tap water with and without NaClO under different temperature conditions through an electrochemical measurement and long-term immersion test. It is anticipated that this research will provide basic information on the application of copper in hot water environments, such as gas water heaters.

## 2. Materials and Methods

### *2.1. Material and Test Solution*

The experimental material is a commercial phosphorus deoxidized copper (TP2) plate with a thickness of about 0.5 mm, whose chemical composition (wt%) is 99.90% Cu and 0.01% impurity. The specimens were cut into a size of 10 mm × 10 mm for electrochemical measurements or 20 mm × 30 mm for a long-term immersion test. The working surface was ground with 1000-grit SiC sandpaper and cleaned with distilled water and anhydrous ethanol.

According to the literature [21], synthetic tap water was prepared with (mg $L^{-1}$): $Cl^-$ 80, $SO_4^{2-}$ 90, $HCO_3^-$ 190, $Ca^{2+}$ 70, and $Mg^{2+}$ 22. The pH value was adjusted to 7.6 by dilute $H_2SO_4$ solution. For a simple comparison, 3 ppm NaClO (slightly higher than the limit of the standard GB 5749-2022 [11]) was added into the solution for parallel tests.

### *2.2. Electrochemical Measurements*

Electrochemical measurements were conducted in a typical three-electrode cell with an AMETEK PMC1000 Potentiostat/Galvanostat made in Slovakia and the Powersuite software 2011. Specimen, platinum electrode, and saturated calomel electrode (SCE) were used as the working electrode, auxiliary electrode, and reference electrode, respectively. The solution temperatures were controlled by a water bath at 25, 40, 50, 65, and 80 °C.

The corrosion potential ($E_{corr}$) was measured for 2 h from the beginning of immersion in the test solution. The polarization curve was determined from −0.4 V vs. $E_{corr}$ with a rate of 20 mV $min^{-1}$ until the current density reached 100 mA $cm^{-2}$. The electrochemical measurement was repeated at least three times with different specimens to ensure reliability.

### *2.3. Immersion Test*

Three rectangle specimens (20 mm × 30 mm) were completely immersed in 300 mL test solutions with and without 3 ppm NaClO for 70 d. For each day, the solution temperature was controlled by a water bath at 25, 40, 50, 65, and 80 °C for 12 h in the daytime and at room temperature for 12 h in the nighttime. The test solutions were renewed once a day. Before the immersion, the specimen surfaces were ground with 1000# SiC abrasive papers, and then rinsed with distilled water and dried with cold air. The size and weight of each specimen were recorded by a vernier caliper and analytical balance.

After 70 d of static immersion in the test solution, the specimens were taken out and cleaned carefully with a brush to remove loose corrosion products on the surface. Pickling was subsequently carried out in dilute sulfuric acid solution for 3 min to remove the corrosion products on the specimens. Ultimately, the specimens were weighed again to calculate the corrosion rate by the following:

$$Vcorr = \frac{m_1 - m_2}{S.t} \quad (1)$$

where $V_{corr}$ is the weight loss rate of copper in mg $m^{-2}$ $d^{-1}$, $m_1$ and $m_2$ are the weights before and after the immersion test in mg, $S$ is the surface area of the specimen in $m^2$, and $t$ is the immersion time in day (d).

### *2.4. Surface Analysis*

After the immersion test, the specimen surface was analyzed by Gemini300 scanning electron microscopy (SEM) with energy-dispersive X-ray spectroscopy (EDS) from Carl Zeiss AG in Oberkochen, Germany. The composition of corrosion products on the specimen was analyzed with X-ray diffraction (XRD) by using a Rigaku diffractometer (D/MAX 2550 V, Tokyo, Japan) with Cu Ka irradiation (λ = 0.15405 nm). The scanning rate was 4° per minute for 2$\theta$ ranging from 10° to 90°. The super depth of a field three-dimensional microscope (Olympus DSX-510, Tokyo, Japan) with 1000× magnification was used to observe the surface morphology and the pit cross-sectional morphology of the specimen and measure the pit depth. The average depth was calculated with the 10 deepest pits according to the International Standard ISO 11463:2020 [22].

## 3. Results

### *3.1. Potentiodynamic Polarization Measurements*

Figure 1 shows the potentiodynamic polarization curves of copper in synthetic tap water at different temperatures. The polarization curves have similar characteristics at different temperatures. All specimens are in active corrosion state. In the weak polarization region ($E < 0.1$ $V_{SCE}$), the anodic current density shows insignificant difference at a temperature lower than 50 °C and noticeably decreases with temperature from 50 to 80 °C. In the very strong polarization region ($E > 0.3$ $V_{SCE}$), the anodic current density increases with temperature from 25 to 50 °C and displays almost no variation at temperatures higher than 50 °C. The cathodic current density gradually increases with temperature from 25 to 65 °C and slightly decreases with temperature from 65 to 80 °C. For example, the cathode current densities at −0.3 $V_{SCE}$ are 8.5, 8.9, 10.8, 18.2, and 16.8 μA $cm^{-2}$ for temperatures from 25 to 80 °C, which show a turning point at 65 °C. It is noted that there is an oxygen diffusion feature to some extent in the cathodic polarization process, especially under temperatures of 65 and 80 °C.

Figure 2 shows the potentiodynamic polarization curves of copper in synthetic tap water with the addition of 3 ppm NaClO at different temperatures. The anodic current density in the weak polarization region ($E < 0.1$ $V_{SCE}$) reaches the largest values at 40 °C and significantly decreases with the further increase in temperature. At higher potentials ($E > 0.3$ $V_{SCE}$), the current density is relatively small at 25 °C and displays very small variation at temperatures above 40 °C. The cathodic current density gradually enlarges with the solution temperature, but shows a very small difference for temperatures of 65 and 80 °C. For instance, the cathode current densities at −0.3 $V_{SCE}$ were 8.9, 11.4, 14.2, 19.2, and 21.1 μA $cm^{-2}$ for solution temperatures from 25 to 80 °C.

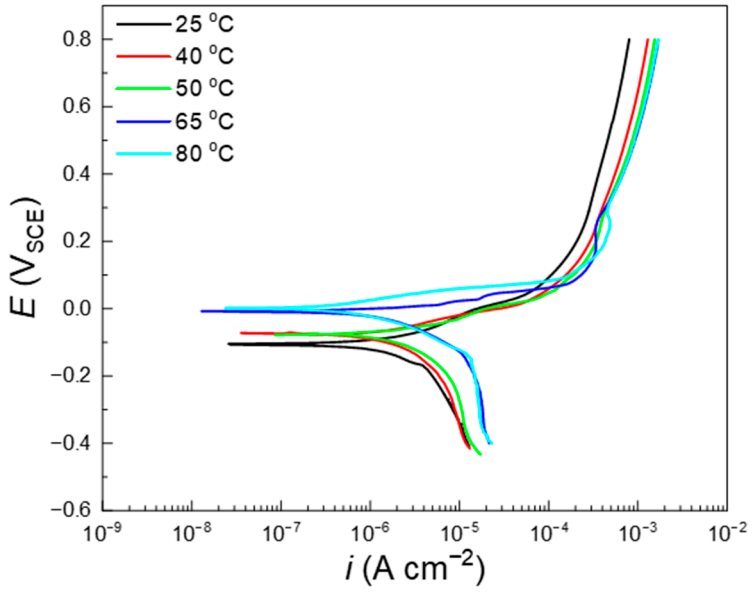


**Figure 1.** Potentiodynamic polarization curves for the specimens in synthetic tap water at different temperatures.

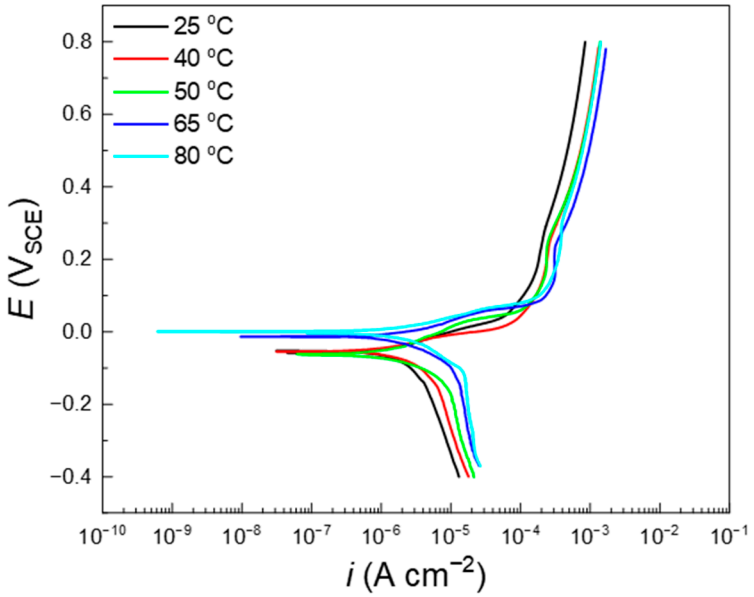


**Figure 2.** Potentiodynamic polarization curves for the specimens in synthetic tap water with 3 ppm NaClO at different temperatures.

### *3.2. Optical Morphology*

Figure 3 shows macroscopic images of the specimen surfaces immersed in synthetic tap water with and without NaClO at different temperatures for 70 d. As shown in Figure 3a–e for synthetic tap water without NaClO, all specimen surfaces almost have no metallic luster after the immersion corrosion. For the solutions at 25 °C to 50 °C, there are mainly reddish brown and green corrosion products formed on the surfaces. The green corrosion products significantly grow with the increase in temperature. For the immersion at 65 and 80 °C, the specimen surfaces are completely covered by the brownish black corrosion products.

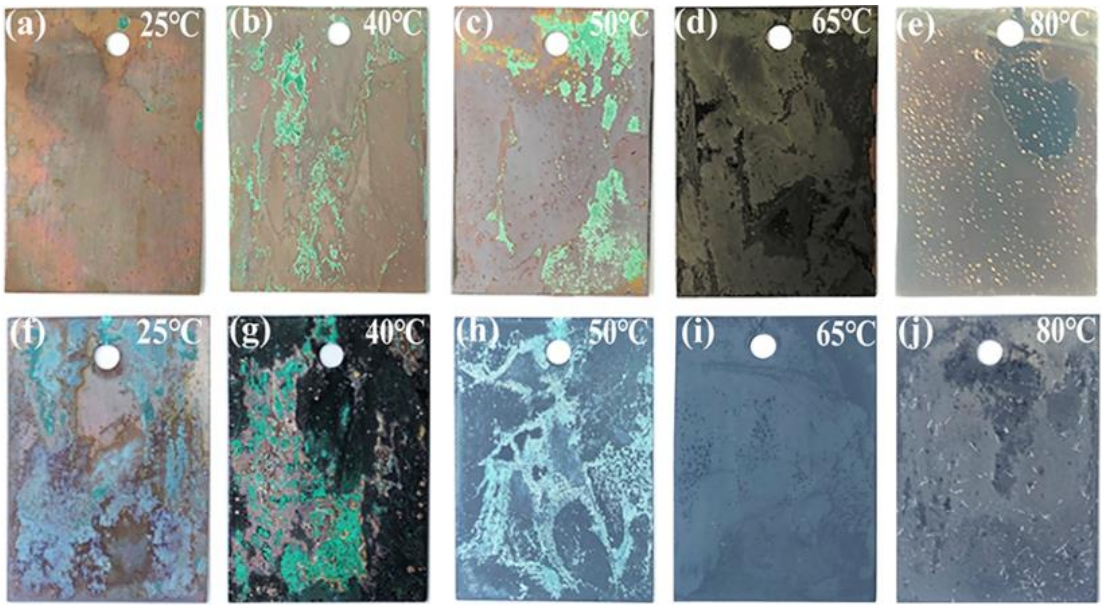


**Figure 3.** Macroscopic surface images for the specimen immersed in synthetic tap water (**a**–**e**) without and (**f**–**j**) with 3 ppm NaClO at different temperatures for 70 d.

After being immersed in synthetic tap water with 3 ppm NaClO at 25 °C for 70 d, as shown in Figure 3f–j, the specimen surfaces display dark brown and green corrosion products without any metallic luster. As the solution temperature is higher than 40 °C, especially 65 °C, the surface basically turns black, with the appearance of a very small amount of green corrosion products. A simple comparison indicates that the addition of 3 ppm NaClO into the solution produces more corrosion products and then a significantly darker surface for the specimen under each temperature condition.

Figure 4 gives the local optical morphologies of pits on the specimens immersed in the two solutions at different temperatures for 70 d. In synthetic tap water without NaClO, as shown in Figure 4a–e, the pits are covered with green corrosion products. The pits significantly enlarge with the change in temperature from 25 to 50 °C, but are difficult to be observed due to their small sizes for temperatures at 65 °C and 80 °C. In synthetic tap water with NaClO, as shown in Figure 4f–j, the green corrosion products appear above the big pits on the specimen surfaces for temperatures at 25 °C and 40 °C. There are also many small pits. Under the conditions of 50 °C to 80 °C, only very small corrosion pits can be observed on the black specimen surfaces.

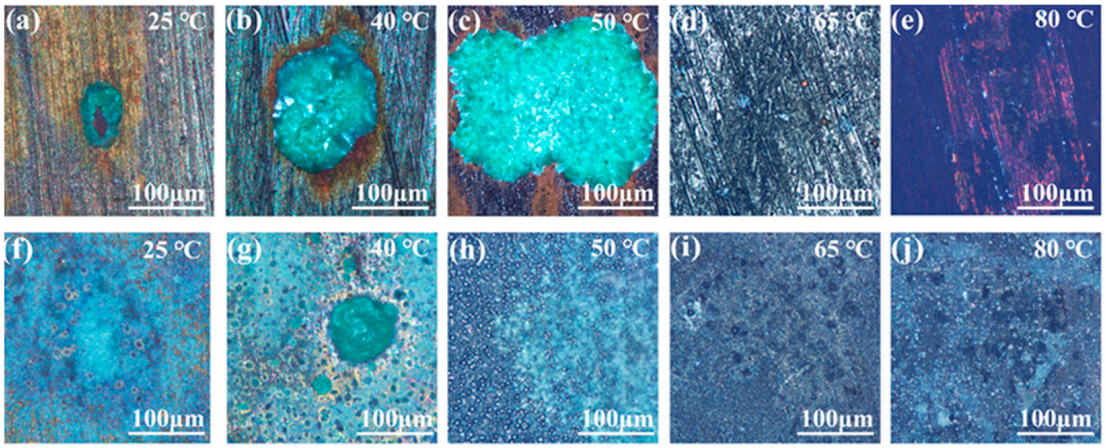


**Figure 4.** Local optical images for the corrosion pits on the specimen surfaces after immersion in synthetic tap water (**a**–**e**) without and (**f**–**j**) with 3 ppm NaClO at different temperatures.

### *3.3. Characterization of Corrosion Products*

Figure 5 gives typical SEM images of corrosion products on the specimen surfaces after the immersion test in synthetic tap water at 50 and 65 °C. For the specimen surface at 50 °C, the reddish brown area displays a relative corrosion product layer in Figure 5a, which is mainly composed of blocky and spherical product particles [23]. The green area shows a relatively loose and porous product layer in Figure 5b, which mainly consists of lamellar flakes. The corrosion products on the specimen surfaces at 25 and 40 °C are basically similar to those at 50 °C. For the specimen at 65 °C, the black corrosion product layer exhibits acicular characteristics in Figure 5c. The corrosion products on the specimen at 80 °C are similar to those at 65 °C.

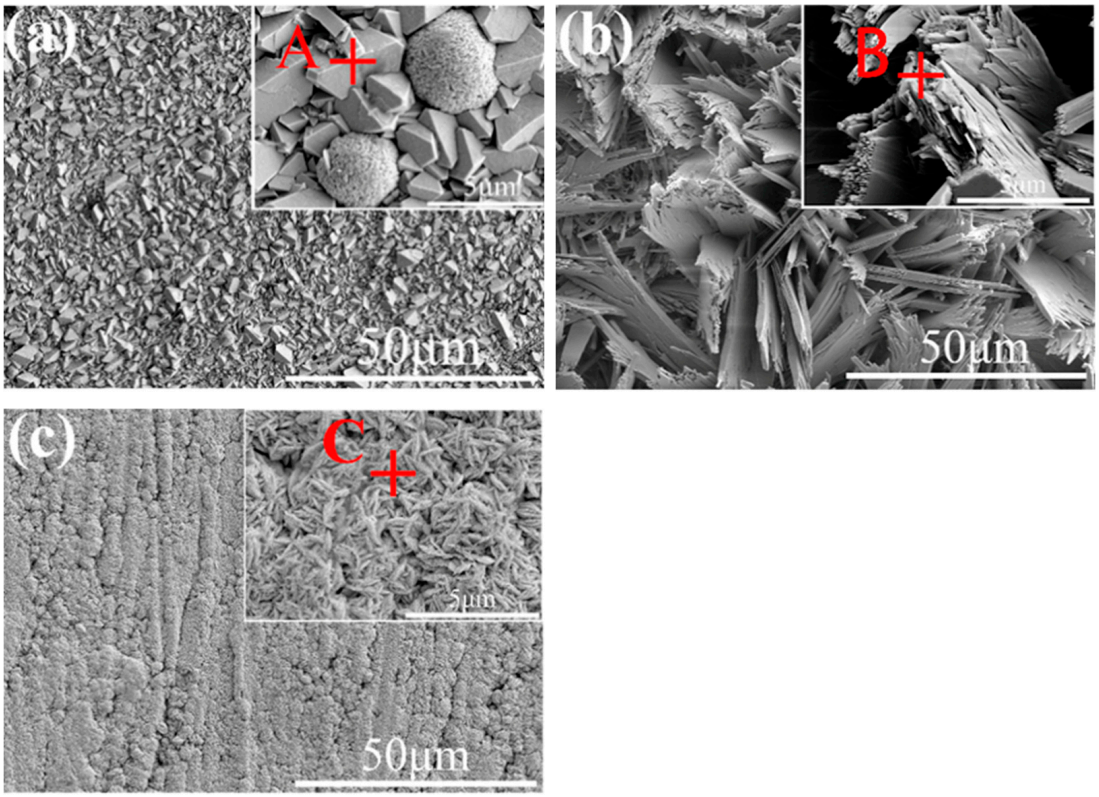


**Figure 5.** SEM images of the specimen surfaces after immersion in synthetic tap water at different temperatures: (**a**,**b**) 50 °C and (**c**) 65 °C.

Figure 6 gives typical SEM images of corrosion products on the specimen surfaces after the immersion test in synthetic tap water with 3 ppm NaClO at different temperatures. Figure 6a,b show that the reddish brown and green corrosion products exhibit granular and filamentous characteristics, respectively, on the specimen surface at 40 °C. There are some micropores in the corrosion product layer. The corrosion products on the specimen surface at 25 °C are basically similar to those at 40 °C. Figure 6c,d show that the black and green corrosion products are irregularly spherical and lath-like on the specimen surface at 50 °C. Figure 6e,f show that the black corrosion products exhibit spindle-like and granular characteristics on the specimen surfaces at 65 and 80 °C, respectively.

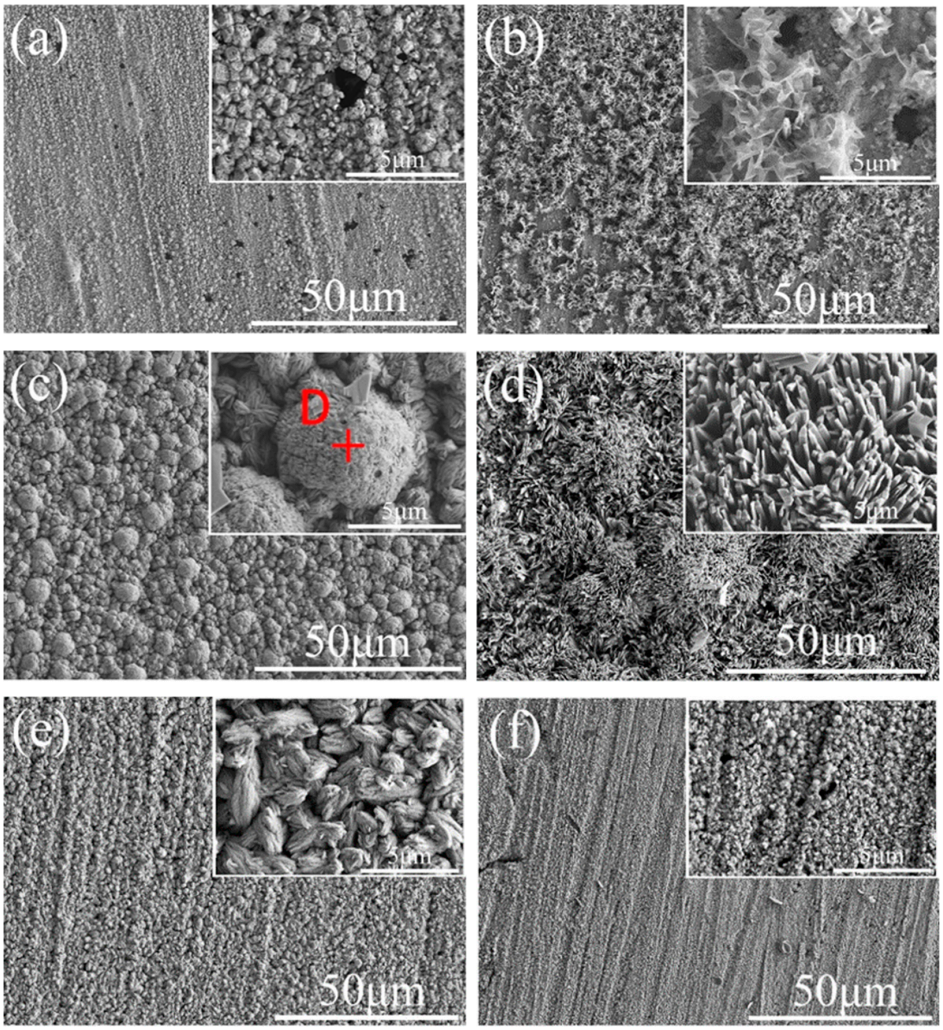


**Figure 6.** SEM images of the specimen surfaces after immersion in synthetic tap water with 3 ppm NaClO at different temperatures: (**a**,**b**) 40 °C, (**c**,**d**) 50 °C, (**e**) 65 °C, and (**f**) 80 °C.

Table 1 gives the EDS analysis results of element contents for the selected products in Figures 5 and 6. The elemental composition of corrosion products in each region mainly consists of Cu, C, and O. Combined with the optical and SEM morphologies, it can be inferred that the reddish brown product at position A is mainly $Cu_2O$, the green product at position B is $Cu_2(OH)_2CO_3$, and the black acicular and spherical products at positions C and D are mainly CuO.

**Table 1.** EDS results for element content (wt.%) at the positions marked in Figures 5 and 6.

| Position | C | O | Cu |
|---|---|---|---|
| A | 0.5 | 8.9 | 90.6 |
| B | 5.1 | 38.3 | 56.6 |
| C | 1.4 | 21.7 | 76.9 |
| D | 1.8 | 21.5 | 76.7 |

Figure 7 gives the XRD spectra for the specimens immersed in synthetic tap water with and without 3 ppm NaClO at different temperatures for 70 d. The corrosion products formed in both solutions are mainly composed of $Cu_2O$, CuO, and $Cu_2(OH)_2CO_3$, which is consistent with EDS analysis. Overall, it is seen from the response peaks (e.g., 31.2, 36.5, and 38.9) that, in the absence and presence of NaClO, the diffraction intensities of $Cu_2O$ and $Cu_2(OH)_2CO_3$ are relatively stronger at temperatures below 50 and 40 °C, respectively.

Their response peaks become significantly weaker at higher solution temperatures. The CuO response peak significantly enhances with the solution temperature rising to 65 and 50 °C in the absence and presence of NaClO, respectively. The variation of peak intensity for CuO is opposite to those for $Cu_2O$ and $Cu_2(OH)_2CO_3$ with temperature. These results indicate that the predominant corrosion products are $Cu_2O$ and $Cu_2(OH)_2CO_3$ below 50 and 40 °C on the specimen surfaces in synthetic tap water without and with 3 ppm NaClO, but it changes to CuO at higher solution temperatures. It is noted that all corrosion products display extremely weak response peaks at 80 °C because their quantities are very small. These are consistent with the observations in Figures 3 and 4.

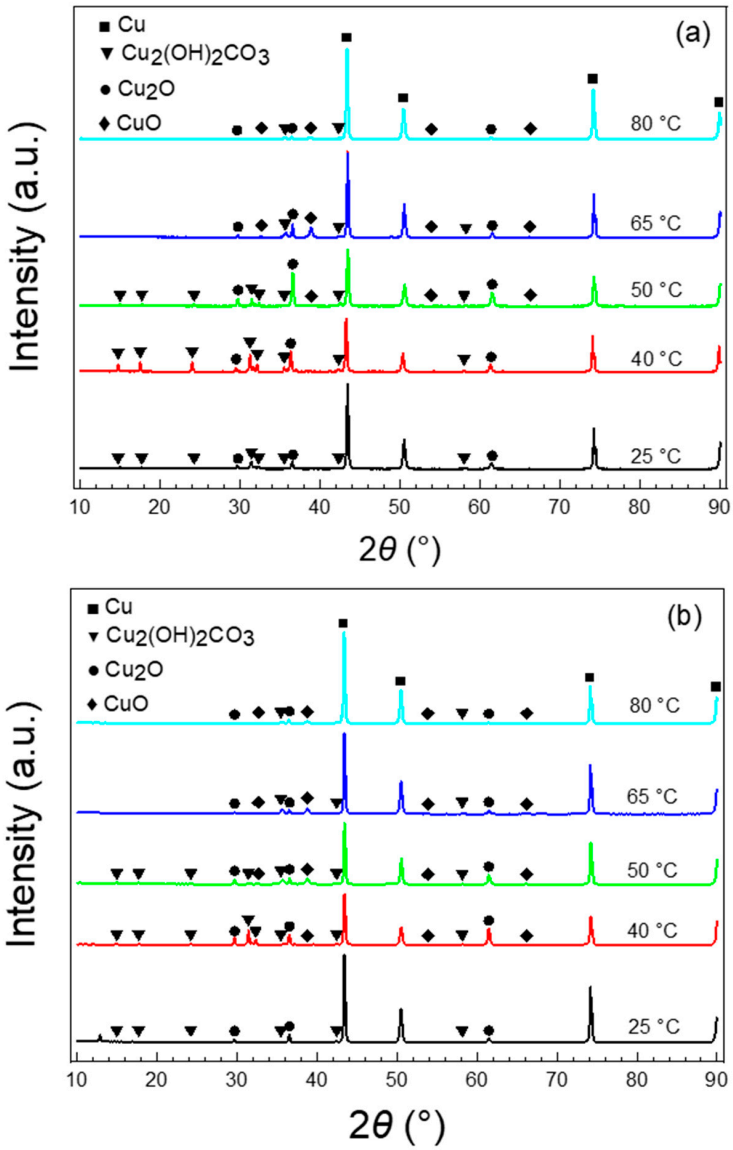


**Figure 7.** XRD patterns for the specimens immersed in synthetic tap water (**a**) without and (**b**) with 3 ppm NaClO at different temperatures.

### *3.4. Pit Observation*

Figure 8 shows typical SEM morphologies of corrosion pits on the pickled specimen surfaces after the immersion test in synthetic tap water at different temperatures. Overall, the corrosion pits formed at different temperatures are shallow and small, exhibiting ulcerative features. Compared with 25, 65, and 80 °C, the specimens display slightly larger corrosion pits after the immersion corrosion at 40 and 50 °C. In addition, all specimens have a certain degree of uniform corrosion over the whole surfaces.

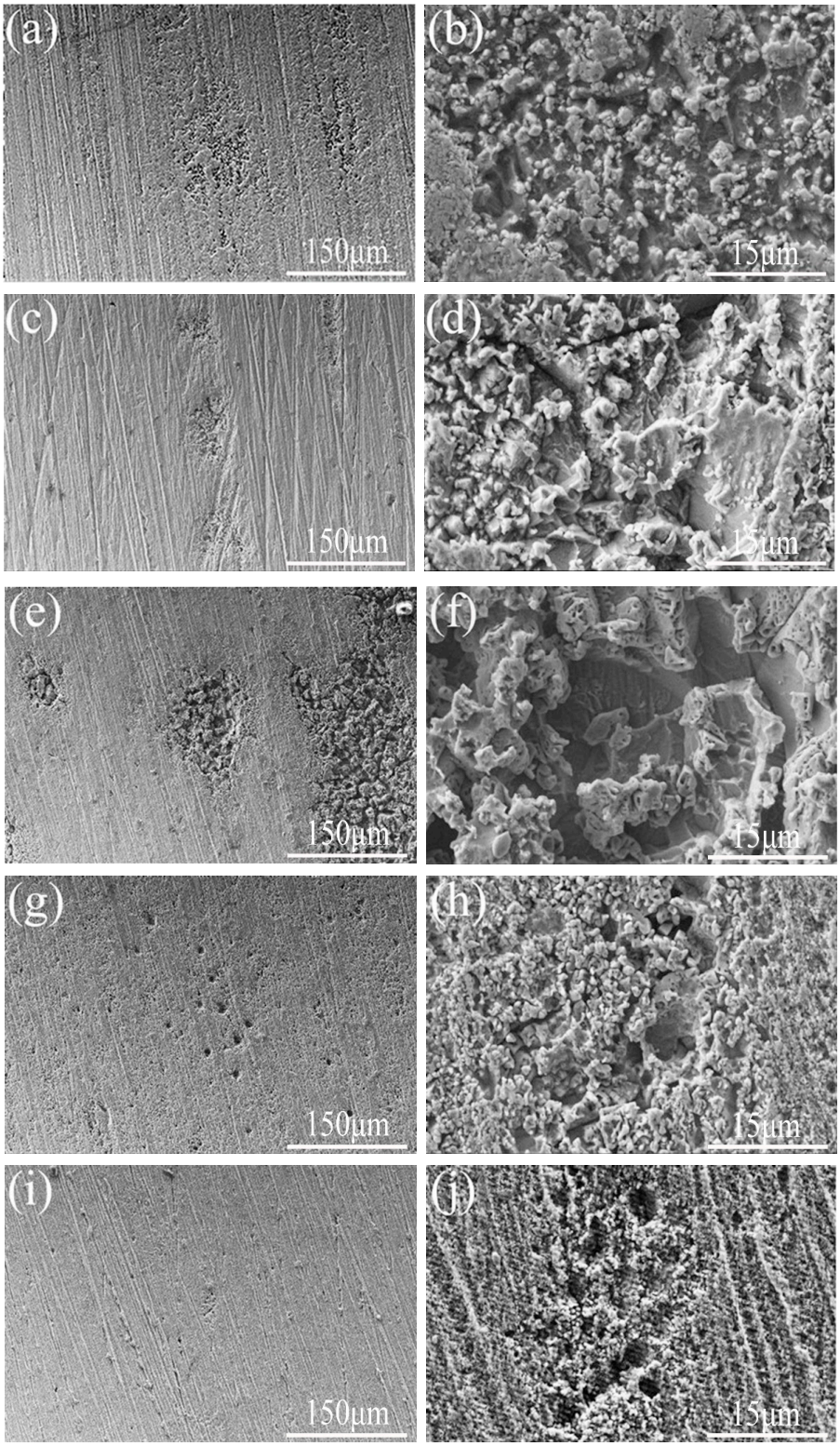


**Figure 8.** Typical SEM morphologies of pits on the pickled specimen surfaces after the immersion test in synthetic tap water at different temperatures: (**a**,**b**) 25 °C, (**c**,**d**) 40 °C, (**e**,**f**) 50 °C, (**g**,**h**) 65 °C, and (**i**,**j**) 80 °C.

Figure 9 shows typical SEM morphologies of pits on the pickled specimen surfaces after the immersion test in the synthetic tap water solution with 3 ppm NaClO at different temperatures. The corrosion features are similar to those in NaClO-free solutions in Figure 8, but the ulcerative corrosion is relatively more severe under each temperature.

Some relatively larger corrosion pits appear on the specimen surfaces immersed at 25 and 40 °C, whereas the corrosion becomes more uniform over the whole surface in the solutions above 50 °C and produces many small corrosion pits.

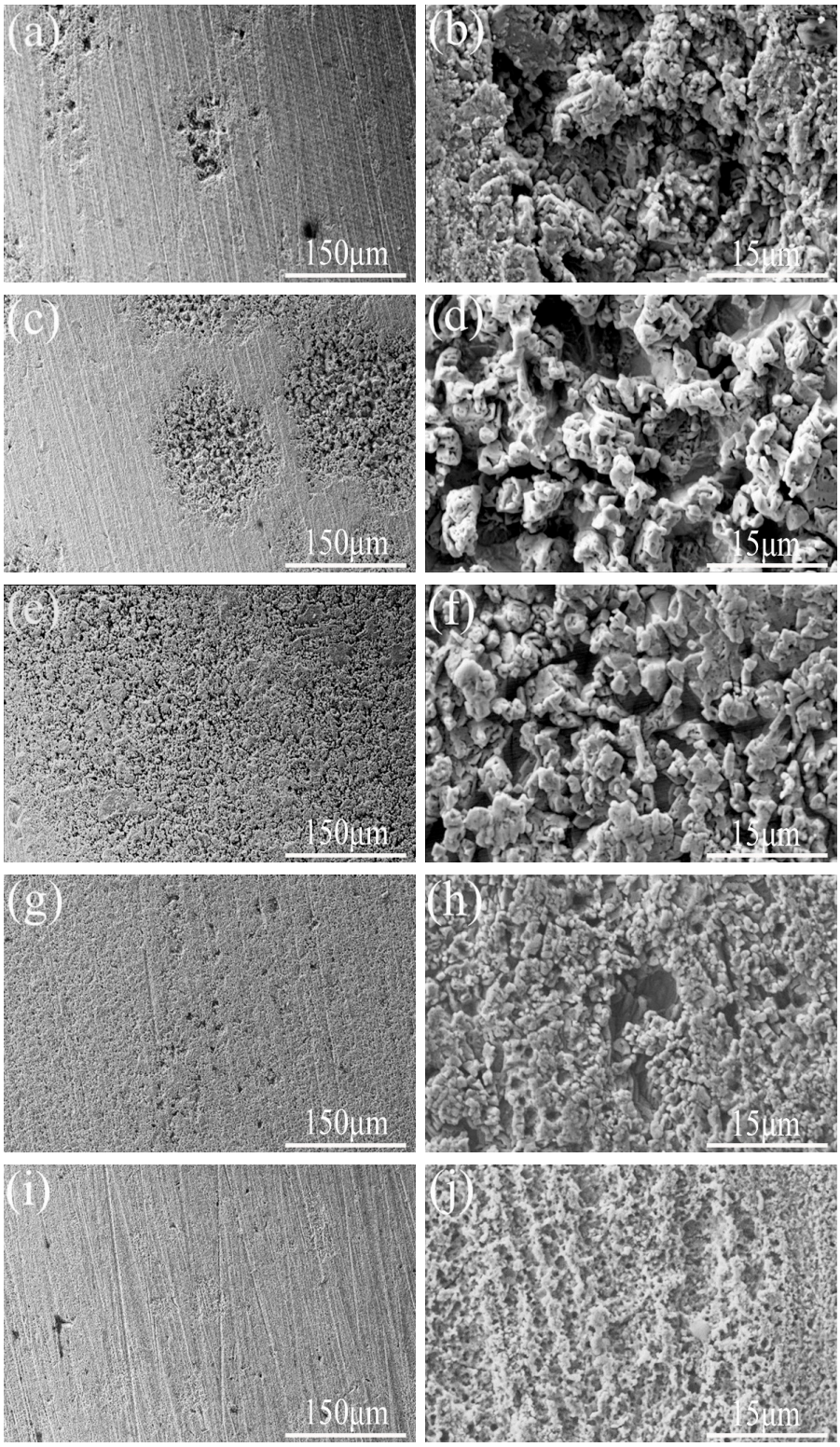


**Figure 9.** Typical SEM morphologies of pits on the pickled specimen surfaces after the immersion test in synthetic tap water with 3 ppm NaClO at different temperatures: (**a**,**b**) 25 °C, (**c**,**d**) 40 °C, (**e**,**f**) 50 °C, (**g**,**h**) 65 °C, and (**i**,**j**) 80 °C.

### *3.5. Corrosion Rate*

Figure 10 gives the weight loss corrosion rates of the specimens after the immersion tests in synthetic tap water with and without 3 ppm NaClO at different temperatures. The corrosion rate exhibits similar evolution characteristics with the temperature for the specimens in the two solutions. The corrosion rate increases at first and then decreases with the increase in temperature, but reaches the maximum values of 206.5 and 246.8 mg $m^{-2}$ $d^{-1}$, respectively, at temperatures of 40 and 50 °C in synthetic tap water with and without NaClO. In addition, the addition of 3 ppm NaClO into synthetic tap water accelerates the corrosion rate of copper to a certain extent under each temperature except for 50 °C. For instance, the corrosion rate exhibits the greatest variation of about 86.5% at 25 °C.

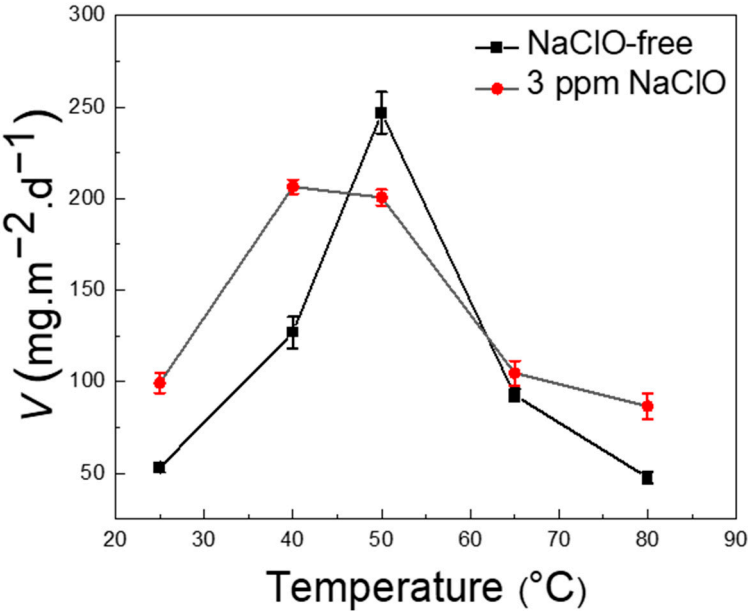


**Figure 10.** Corrosion rate of the specimens immersed in synthetic tap water without and with 3 ppm NaClO at different temperatures.

### *3.6. Pit Depth*

Figure 11 gives the average pit depth values for the specimens after the immersion tests in synthetic tap water with and without 3 ppm NaClO at different temperatures. The pit depth also displays similar evolution characteristics with the temperature in the two solutions. In NaClO-free synthetic tap water, the pit depth slightly enlarges from 3.5 to 15.1 μm with the change in temperature from 25 to 50 °C, and then rapidly reduces to 2.4 and 1.8 μm, respectively, with the further increase in temperature to 65 and 80 °C. In synthetic tap water with 3 ppm NaClO, the deepest pit is about 11.2 μm at 40 °C, whereas the pit depth decreases from 5.3 to 2.8 μm with the increase in temperature from 50 to 80 °C. The addition of 3 ppm NaClO into the solution slightly deepens the pit depth under each temperature except for 50 °C. Furthermore, it is seen that the pits are very shallow in the two solutions, which have a depth of less than about 15 μm after the immersion corrosion for 70 d under 25 to 80 °C.

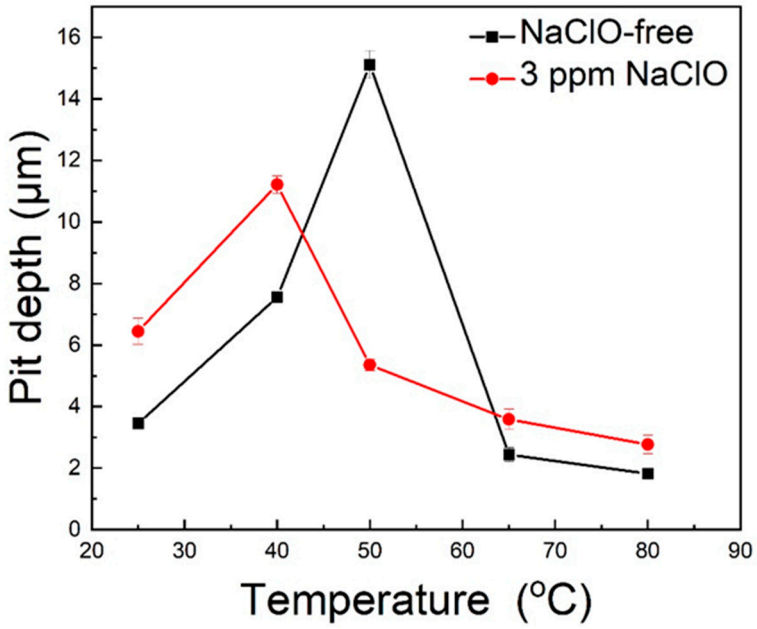


**Figure 11.** Average pit depth for the specimens after the immersion tests in synthetic tap water without and with 3 ppm NaClO at different temperatures.

## 4. Discussion

### *4.1. Corrosion Mechanism under Different Temperatures*

The polarization curves in Figure 1 indicate that oxygen reduction is the cathodic reaction of the corrosion process on the specimen surface in synthetic tap water [24,25], as shown in the following equation:

$$O_2 + 2H_2O + 4e \rightarrow 4OH^- \quad (2)$$

When the solution temperature increases from 25 to 65 °C, the cathodic current density at −0.3 $V_{SCE}$ enlarges about 1.1 times. It is well known that a higher temperature may enhance the activation of corrosion reactions and the diffusion of dissolved oxygen [7,9,26]. These may facilitate the oxidation reaction of copper and then accelerate its corrosion in synthetic tap water. However, when the temperature reaches 80 °C, the cathodic current density slightly decreases to 16.8 μA $cm^{-2}$. This can be mainly attributed to the significant reduction in oxygen content in the solution. It is reported that the dissolved oxygen content linearly changes from about 8.0 to 3.5 mg $L^{-1}$ with the increase in temperature from 25 to 80 °C [27], which is unfavorable for the cathodic reaction of the corrosion process.

Figure 1 also shows the reduction in anodic current density in the weak polarization region as the temperature exceeds 50 °C. This is mainly related to the formation of a corrosion product layer on the specimen surface [28]. The corrosion of a fresh copper specimen in tap water rapidly generates $Cu_2O$ on the surface, which has a certain protective effect on the copper matrix [29]. $Cu_2O$ will be further oxidized to form divalent corrosion products such as CuO [30], as shown in the following equations:

$$Cu + H_2O \rightarrow Cu_2O + 2H^+ + 2e \quad (3)$$

$$Cu_2O + H_2O \rightarrow 2CuO + 2H^+ + 2e \quad (4)$$

The dissolved $Cu^{2+}$ ions undergo a secondary reaction with $CO_3^{2-}$, $HCO_3^{2-}$, and $OH^-$ ions in the solution to form $Cu_2(OH)_2CO_3$ on the specimen surface, as shown in the following equation:

$$2Cu^{2+} + 2OH^- + CO_3^{2-} \rightarrow Cu_2(OH)_2CO_3 \quad (5)$$

Figures 3 and 7 indicate that the predominant corrosion products change from $Cu_2O$ and $Cu_2(OH)_2CO_3$ to CuO when the solution temperature is higher than 50 °C. This is consistent with the thermodynamic calculation in the literature [30]. CuO is more protective than $Cu_2(OH)_2CO_3$ to the copper matrix [31,32], which may be mainly responsible for the left shift of anodic polarization curves at 65 and 80 °C in Figure 1. It is clear that the formation of CuO inhibits the anodic process. As shown in Figure 5, the loose $Cu_2(OH)_2CO_3$ layer formed on the specimen surface under temperatures below 50 °C and significantly reduced at higher temperatures. According to Figure 4 and the literature [6,33–35], the corrosion under the green product $Cu_2(OH)_2CO_3$ is prone to produce pits on the copper surface at lower temperatures. During the long-term immersion process, the electrochemical corrosion cell with a small anode and large cathode feature may form along the pits on the specimen surface, which can promote anodic dissolution and the growth of the pits [36,37].

Obviously, increasing the solution temperature has a dual effect on copper corrosion. On the one hand, it can accelerate the cathodic and anodic reactions, i.e., the corrosion process. On the other hand, it may promote the formation of a corrosion product layer with different components and reduce the dissolved oxygen content in tap water, and thus inhibiting the corrosion process. As a result, the mutual constraint between these two aspects leads to the appearance of maximum values of corrosion rate and pitting depth with the increase in solution temperature, as shown in Figures 10 and 11.

### *4.2. Corrosion Mechanism in the Presence of NaClO*

The addition of NaClO will form chlorinated tap water, where free chlorine mainly exists in the form of $ClO^-$ and HClO [13,17]. Both species can act as oxidants participating in the cathodic reaction process like oxygen, as shown in reactions (6) and (7). This is responsible for the enlargement of the cathodic current density for the specimen after the addition of NaClO into the solution under each temperature, as shown in Figure 12.

$$ClO^- + H_2O + 2e \rightarrow Cl^- + 2OH^- \qquad E_{SHE}{}^0 = 0.89\ V \tag{6}$$

$$HClO + H^+ + 2e \rightarrow Cl^- + H_2O \qquad E_{SHE}{}^0 = 1.49\ V \tag{7}$$

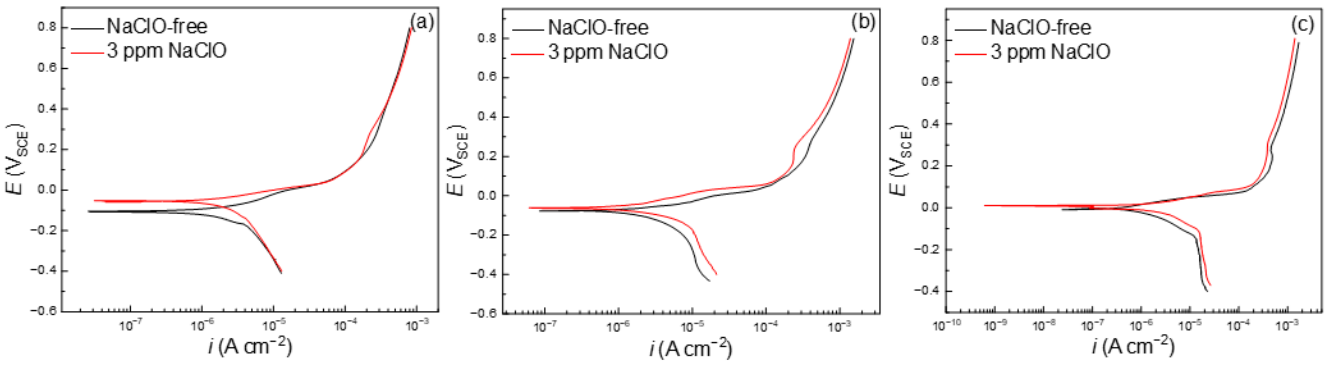


**Figure 12.** Comparisons for the potentiodynamic polarization curves in synthetic tap water without and with 3 ppm NaClO at different temperatures: (**a**) 25 °C, (**b**) 50 °C, and (**c**) 80 °C.

It can be seen from reactions (6) and (7) that, in comparison with oxygen reduction, chlorine reduction in HClO theoretically has a higher oxidation-reduction potential, which may produce a stronger polarization on the anodic dissolution reaction of copper. This leads to the increase in corrosion potential for the specimens in the solution with 3 ppm NaClO at 25 and 40 °C, especially at 25 °C in Figure 12, where the corrosion potential increases from about −0.102 to −0.056 $V_{SCE}$. These effects of NaClO may accelerate the corrosion dissolution and pit growth of copper to a certain extent. Therefore, the weight loss rate and pit depth of the specimens in Figures 10 and 11 become relatively higher in

the presence of 3 ppm NaClO at all temperatures except 50 °C. However, under a solution temperature of 50 °C, NaClO also promotes the transformation of $Cu_2O$ to CuO and the growth of a corrosion product layer by accelerating reactions (3) and (4), as shown in Figure 3. At the same time, the loose green product $Cu_2(OH)_2CO_3$ significantly reduces on the specimen, which is unfavorable for the occurrence of pitting corrosion. Therefore, the addition of 3 ppm NaClO into tap water results in a relatively lower weight loss rate and pit depth at 50 °C. In addition, as the solution temperature reaches 65 and 80 °C, the corrosion potential displays an insignificant difference for the specimens in the two solutions, which is mainly related to the decrease in HClO in the solution. It is noted from Figure 12 that the anodic current density shows a slight decrease in most electrode potential cases with the addition of 3 ppm NaClO, which can be mainly related to the faster formation of corrosion products on the fresh specimen surface. This may differ from the long-term immersion corrosion result in Figure 10.

## 5. Conclusions

The influence of temperature and NaClO on the corrosion behavior of copper was investigated in synthetic tap water. The main conclusions are drawn as follows:

(1) Copper displays active corrosion in synthetic tap water. Corrosion products significantly affect its corrosion resistance. Predominant corrosion products change from $Cu_2O$ and $Cu_2(OH)_2CO_3$ to CuO as the solution temperature is higher than 50 °C. Compared with the loose $Cu_2(OH)_2CO_3$, CuO exhibits stronger inhibition on the anodic corrosion process. With the increase in solution temperature, the weight loss rate and pit depth slightly enlarge before reaching a maximum value at 50 °C.

(2) The addition of 3 ppm NaClO into the solution accelerates the cathodic reaction rate and then, to some extent, increases the weight loss rate and pit depth of copper at various temperatures except for 50 °C. The maximum weight loss rate and pit depth appear at 40 °C with the increase in solution temperature because the main corrosion products on the specimen surface change from $Cu_2O$ and $Cu_2(OH)_2CO_3$ to CuO above 40 °C.

**Author Contributions:** Conceptualization, M.L. and F.S.; validation, N.Z. and S.C.; formal analysis, F.S., N.Z. and S.C.; investigation, F.S.; resources, M.L.; data curation, F.S and N.Z.; writing—original draft preparation, F.S.; writing—review and editing, M.L.; visualization, S.C.; supervision, M.L. All authors have read and agreed to the published version of the manuscript.

**Funding:** This research received no external funding.

**Data Availability Statement:** Data are contained within the article.

**Acknowledgments:** F.S. thanks Yong Yang and Sensen Xin (Midea Group) for the useful discussions.

**Conflicts of Interest:** The authors declare no conflicts of interest.

## References

1. Zhang, Z.; Zheng, C.; Yi, G.; Zhang, C.; Qi, H. Investigation on the Electrochemical Corrosion Behavior of TP2 Copper and Influence of BTA in Organic Acid Environment. *Metals* **2022**, *12*, 1629. [CrossRef]
2. Lytle, D.A.; Schock, M.R.; Leo, J.; Barnes, B. A model for estimating the impact of orthophosphate on copper in water. *J. Am. Water Work Assoc.* **2018**, *110*, E1–E15. [CrossRef] [PubMed]
3. Hedin, A.; Johansson, A.J.; Lilja, C.; Boman, M.; Berastegui, P.; Berger, R.; Ottosson, M. Corrosion of copper in pure $O_2$-free water? *Corros. Sci.* **2018**, *137*, 1–12. [CrossRef]
4. Ottosson, M.; Boman, M.; Berastegui, P.; Andersson, Y.; Hahlin, M.; Korvela, M.; Berger, R. Copper in ultrapure water, a scientific issue under debate. *Corros. Sci.* **2017**, *122*, 53–60. [CrossRef]
5. Shalaby, H.M.; Al-Kharafi, F.M.; Gouda, V.K.J.; Tx, H. A Morphological Study of Pitting Corrosion of Copper in Soft Tap Water. *Corros. Sci.* **1989**, *45*, 536–547. [CrossRef]
6. Lytle, D.A.; Nadagouda, M.N. A comprehensive investigation of copper pitting corrosion in a drinking water distribution system. *Corros. Sci* **2010**, *52*, 1927–1938. [CrossRef]
7. Rahman, M.M.; Ahmed, S.R. Corrosion behavior of copper based heat exchanger tube in waters of Bangladesh region at varied temperature and flow velocity. *Maejo Int. J. Sci. Technol.* **2020**, *8*, 15–23. [CrossRef]

8. Ren, L.; Cheng, Y.; Wang, Q.; Tian, X.; Yang, J.; Zhang, D. Relationship between corrosion product and fouling growth on mild steel, copper and brass surface. *Colloid Surf. A-Physicochem. Eng. Asp.* **2020**, *591*, 124502. [CrossRef]
9. Cai, Y.K.; Xu, Y.M.; Zhao, Y.; Zhang, W.F.; Yao, J.H.; Wei, M.M.; Zhou, K.; Ma, X.B. Quantitative Understanding of the Environmental Effect on B10 Copper Alloy Corrosion in Seawater. *Metals* **2021**, *11*, 1080. [CrossRef]
10. Li, B.; Liu, R.; Liu, H.; Gu, J.; Qu, J. The formation and distribution of haloacetic acids in copper pipe during chlorination. *J. Hazard. Mater.* **2008**, *152*, 250–258. [CrossRef]
11. *GB5749–2022*; Standards for Drinking Water Quality. SAMR and SA: Beijing, China, 2022.
12. Montes, J.C.; Hamdani, F.; Creus, J.; Touzain, S.; Correc, O. Impact of chlorinated disinfection on copper corrosion in hot water systems. *Appl. Surf. Sci.* **2014**, *314*, 686–696. [CrossRef]
13. Cong, H.B.; Scully, J.R. Effect of Chlorine Concentration on Natural Pitting of Copper as a Function of Water Chemistry. *J. Electrochem. Soc.* **2010**, *157*, C200–C211. [CrossRef]
14. Ives, M.B.; Lu, Y.C.; Luo, J.L. Cathodic reactions involved in metallic corrosion in chlorinated saline environments. *Corros. Sci.* **1991**, *32*, 91–102. [CrossRef]
15. Suzuki, I.; Ishikawa, Y.; Hisamatsu, Y. The pitting corrosion of copper tubes in hot water. *Corros. Sci.* **1983**, *23*, 1095–1106. [CrossRef]
16. Reiber, S.H. Copper plumbing surfaces: An electrochemical study. *J. Am. Water Work Assoc.* **1989**, *81*, 114–122. [CrossRef]
17. Atlas, D.; Coombs, J.; Zajicek, O.T. The corrosion of copper by chlorinated drinking waters. *Water Res.* **1982**, *16*, 693–698. [CrossRef]
18. Boulay, N.; Edwards, M. Role of temperature, chlorine, and organic matter in copper corrosion by-product release in soft water. *Water Res.* **2001**, *35*, 683–690. [CrossRef] [PubMed]
19. Yohai, L.; Schreiner, W.; Vázquez, M.; Valcarce, M. Brass corrosion in chlorinated tap water inhibited by phosphate ions. *J. Solid State Electrochem.* **2015**, *19*, 1559–1568. [CrossRef]
20. Tzevelekou, T.; Flampouri, A.; Rikos, A.; Vazdirvanidis, A.; Pantazopoulos, G.; Skarmoutsos, D. Hot-water corrosion failure of a hard-drawn copper tube. *Eng. Fail. Anal.* **2013**, *33*, 176–183. [CrossRef]
21. Xian, W.; Yin, Z.; Liu, L.; Li, M. Electrochemical Corrosion Behavior of 310S Stainless Steel in Hot Concentrated Tap Water. *Metals* **2023**, *13*, 713. [CrossRef]
22. Duan, T.; Peng, W.; Ding, K.; Zhao, Y.; Hou, J.; Cheng, W.; Xu, L. Long-term localized corrosion behaviors of 5A06 aluminum alloys exposed in the natural deep-sea environment of South China Sea. *J. Mater. Res. Technol.* **2022**, *20*, 4597–4607. [CrossRef]
23. Sun, S.; Zhang, X.; Yang, Q.; Liang, S.; Zhang, X.; Yang, Z. Cuprous oxide ($Cu_2O$) crystals with tailored architectures: A comprehensive review on synthesis, fundamental properties, functional modifications and applications. *Prog. Mater. Sci.* **2018**, *96*, 111–173. [CrossRef]
24. Lee, Y.-H.; Byun, J.-H.; Ko, S.-J.; Park, E.-H.; Kim, J.-G. Effect of oxygen on pitting corrosion of copper pipe in fire sprinkler system. *Mater. Chem. Phys.* **2023**, *301*, 127584. [CrossRef]
25. Zhu, Y.H.; Wang, J.Z.; Liu, H.; Ren, P.W.; Yan, F.Y. Effect of Dissolved Oxygen Content on Tribo-Corrosion Behavior of Monel 400 Alloy in Seawater. *Metals* **2024**, *14*, 6. [CrossRef]
26. Xu, P.; Fu, Q.; Zhao, M. The influence of calcium on copper corrosion and its by-product release in drinking water. *RSC Adv.* **2023**, *13*, 17842–17855. [CrossRef] [PubMed]
27. Zhang, M.; Xu, R.; Liu, L.; Xin, S.; Li, M. Electrochemical corrosion behavior of type 444 stainless steel in synthetic tap water at different temperatures. *Anti-Corros. Methods Mater.* **2020**, *67*, 407–414. [CrossRef]
28. Ives, D.J.G.; Rawson, A.E. Copper corrosion: III. electrochemical theory of general corrosion. *J. Electrochem. Soc.* **1962**, *109*, 458. [CrossRef]
29. Mohammed, A.M.; Mohtar, S.S.; Aziz, F.; Mhamad, S.A.; Aziz, M. Review of various strategies to boost the photocatalytic activity of the cuprous oxide-based photocatalyst. *J. Environ. Chem. Eng.* **2021**, *9*, 105138. [CrossRef]
30. Adeloju, S.B.; Hughes, H.C. The corrosion of copper pipes in high chloride-low carbonate mains water. *Corros. Sci.* **1986**, *26*, 851–870. [CrossRef]
31. Feng, Y.; Teo, W.K.; Siow, K.S.; Tan, K.L.; Hsieh, A.K. The corrosion behaviour of copper in neutral tap water. Part I: Corrosion mechanisms. *Corros. Sci.* **1996**, *38*, 369–385. [CrossRef]
32. Wang, T.; Wang, Y.; Jia, X.; Ye, C. Corrosion failure analysis of hollow copper coil used in generator internal cooling water system operated at low-oxygen/neutral water chemistry. *Eng. Fail. Anal.* **2022**, *141*, 106642. [CrossRef]
33. Ha, H.; Taxen, C.; Williams, K.; Scully, J. Effects of selected water chemistry variables on copper pitting propagation in potable water. *Electrochim. Acta* **2011**, *56*, 6165–6183. [CrossRef]
34. Myers, J.R.; Cohen, A. Pitting corrosion of copper in cold potable water systems. *Mater. Perform.* **1995**, *34*, 60–62.
35. Adeloju, S.B.; Duan, Y.Y. Influence of bicarbonate ions on stability of copper oxides and copper pitting corrosion. *Br. Corros. J.* **1994**, *29*, 315–320. [CrossRef]

36. Lee, Y.-H.; Hong, M.-S.; Ko, S.-J.; Kim, J.-G. Effect of benzotriazole on the localized corrosion of copper covered with carbonaceous residue. *Materials* **2021**, *14*, 2722. [CrossRef] [PubMed]
37. Cong, H.; Michels, H.T.; Scully, J.R. Passivity and Pit Stability Behavior of Copper as a Function of Selected Water Chemistry Variables. *J. Electrochem. Soc.* **2009**, *156*, C16. [CrossRef]

**Disclaimer/Publisher's Note:** The statements, opinions and data contained in all publications are solely those of the individual author(s) and contributor(s) and not of MDPI and/or the editor(s). MDPI and/or the editor(s) disclaim responsibility for any injury to people or property resulting from any ideas, methods, instructions or products referred to in the content.